

Research article

Open Access

Raman and SEM analysis of a biocolonised hot spring travertine terrace in Svalbard, Norway

Susana E Jorge-Villar^{*1,2,3}, Liane G Benning², Howell GM Edwards³ and AMASE team

Address: ¹Area de Geodinámica Interna, Facultad de Humanidades y Educación, C/Villadiego s/n, 09001 Burgos, Spain, ²Earth and Biosphere Institute, School of Earth and Environment, University of Leeds, Leeds, LS2 9JT, UK and ³Chemical and Forensic Sciences, University of Bradford, West Yorkshire BD7 1DP, UK

Email: Susana E Jorge-Villar^{*} - susanajorgevillar@hotmail.com; Liane G Benning - earlgb@earth.leeds.ac.uk; Howell GM Edwards - h.g.m.edwards@bradford.ac.uk; AMASE team - amase@gl.ciw.edu

^{*} Corresponding author

Published: 15 August 2007

Received: 2 February 2007

Geochemical Transactions 2007, 8:8 doi:10.1186/1467-4866-8-8

Accepted: 15 August 2007

This article is available from: <http://www.geochemicaltransactions.com/content/8/1/8>

© 2007 Villar et al; licensee BioMed Central Ltd.

This is an Open Access article distributed under the terms of the Creative Commons Attribution License (<http://creativecommons.org/licenses/by/2.0>), which permits unrestricted use, distribution, and reproduction in any medium, provided the original work is properly cited.

Abstract

Background: A profile across 8 layers from a fossil travertine terrace from a low temperature geothermal spring located in Svalbard, Norway has been studied using both Raman spectroscopy and SEM (Scanning Electron Microscopy) techniques to identify minerals and organic life signals.

Results: Calcite, anatase, quartz, haematite, magnetite and graphite as well as scytonemin, three different carotenoids, chlorophyll and a chlorophyll-like compound were identified as geo- and biosignatures respectively, using 785 and/or 514 nm Raman laser excitation wavelengths. No morphological biosignatures representing remnant microbial signals were detected by high-resolution imaging, although spectral analyses indicated the presence of organics. In contrast, in all layers, Raman spectra identified a series of different organic pigments indicating little to no degradation or change of the organic signatures and thus indicating the preservation of fossil biomarker compounds throughout the life time of the springs despite the lack of remnant morphological indicators.

Conclusion: With a view towards planetary exploration we discuss the implications of the differences in Raman band intensities observed when spectra were collected with the different laser excitations. We show that these differences, as well as the different detection capability of the 785 and 514 nm laser, could lead to ambiguous compound identification. We show that the identification of bio and geosignatures, as well as fossil organic pigments, using Raman spectroscopy is possible. These results are relevant since both lasers have been considered for miniaturized Raman spectrometers for planetary exploration.

Background

There is currently much interest in the detection and characterization of biosignatures in geological environments for planetary exploration; instrumental suites for life detection are being considered for several extreme terres-

trial environments, such as Arctic and Antarctic cold deserts, hypersaline lakes, and for remote robotic surface and subsurface exploration on Mars [1-6].

A combination of analytical techniques is extremely valuable for obtaining complementary information about complex biogeological systems [4,7-11]. In this respect, Raman spectroscopic instrumentation is being evaluated for the adoption of miniaturized versions as part of life detection suites on future Mars missions [12-15]. An important part of this scenario is the acquisition of molecular spectroscopic data signatures from key biomolecules produced as a consequence of extremophile survival in stressed environments; a range of terrestrial Mars analogues have been examined including endoliths, cyanobacteria from meteorite impact craters, stromatolites or volcanic and saline rocks [16-21].

The acquisition of Raman spectral data in conjunction with a surface morphological and an elemental analysis from scanning electron microscopy has a special advantage in that the extraction of biological material from the geological matrix is not necessary and no sample handling or preparation steps are needed; hence, it is possible to obtain direct data on the interactions between organic and inorganic components in a biogeological system. From such data the survival and preservation potential of extremophile biosignatures can be accessed.

From these studies, key Raman biosignatures of organic chemicals produced by organisms in rocks have been established and will be applied here to the study of the remnant biosignatures in a travertine terrace in Svalbard (Norway) using samples collected during the 2004 AMASE (Arctic Mars Analogue Svalbard Expedition) expedition. The combination of scanning electron microscopy and Raman microspectroscopy applied to this biogeological system will facilitate the characterization of morphological and biomolecular data for these Mars analogues for the first time.

Specimens

Samples were collected in the Bockfjorden area of Spitzbergen (Svalbard archipelago, Norway) from the fossil parts of the northernmost warm springs on land, the Troll springs, which are located at N 79 ° 23' and E 13 ° 26'. The springs are linked to the Bockfjorden Volcanic Centre, which is located along a major N-S trending fault-zone separating Devonian red sandstones from Proterozoic basement rocks [22].

The Troll springs are active today only at the topmost end, while the largest part of the terraces created during the lifetime of the springs are now considered fossil remnants of active terraces (Figure 1a). The Troll spring terraces span about 100–120 m in the north south direction and, besides the active pool, they contain many dry, fossil pools of sizes between 2–10 meters. These dry pools often have lips of up to 50 cm in width and draped overflow

edges that can reach several meters in height. The full vertical dimension of the terraces, measured from the today active site and including all the fossil parts varies between 30–50m.

The samples studied here were collected from the draped overhang of an old pool located at the south-easternmost end of the system. This part is considered to be one of the oldest, fossil parts of the Troll terraces (Figure 1b). A traverse consisting of 8 layers with the external, youngest one (layer 1) being underlaid by 7 progressively older layers, was collected and each layer analysed. The thickness of the individual layers varied between 0.7 and 1.8 cm and they exhibited a range of colorations from pure or dirty white to pinkish to slightly greenish or yellow and brown (Figure 1c). Observation of the surrounding rocks showed no indication of any recent water flow except water derived from precipitation. The general appearance of the layers were not indicative of classical cryptoendolithic strata, nor were any clear endolithic or casmolithic signatures observed. However, the slight colouring of certain strata indicated possible endolithic colonization and/or

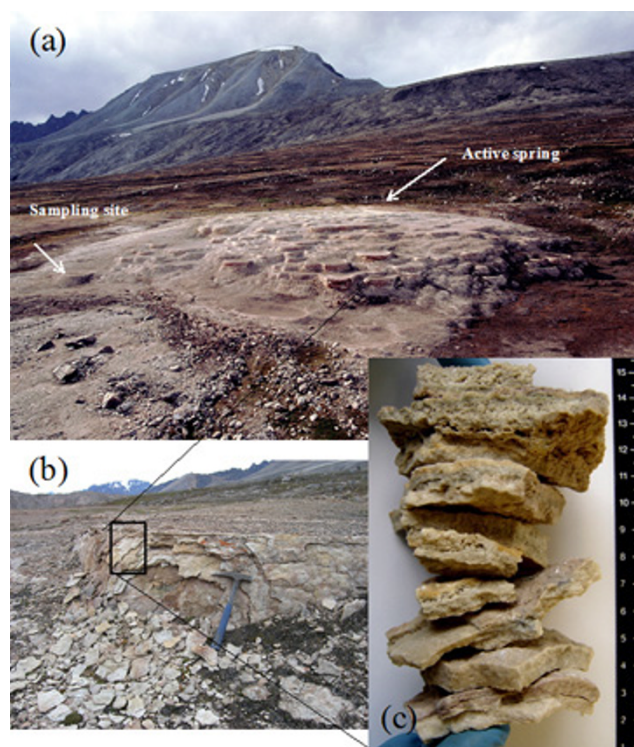


Figure 1
Image of the hotspring, terrace and profile of the analysed layers (a) Overview of the Troll Springs. Indicated are the position of the active part of the spring and the location of the sampling site in the oldest, fossil part of the springs. (b) detailed image of sampling site. (c) Profile of the 8 layers investigated in this study, top young, bottom, old.

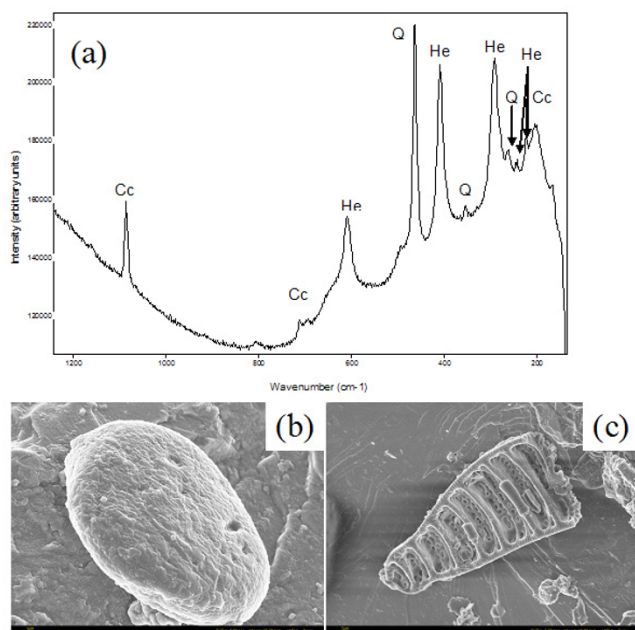


Figure 2
Representative Raman spectrum (a) of quartz (Q), calcite (Cc) and hematite (He) and FEG-SEM images of a dust particle (b) and a diatom (c) recorded at 785 nm laser wavelength. When analyzed using EDS both (c and d) showed Si and O peaks in the spectra. Scales 2 and 1 μ m respectively.

this coloration could be derived from variation in elemental content, i.e. brown, yellow indicating higher iron content or pink indicating higher Mn content [23]. The collected samples were analysed with no further sample preparation and in a consecutive mode with Raman analyses (no sample preparation, except breaking under sterile conditions, flow cabinet) being followed by high-resolution microscopy and elemental analyses (coating and in vacuum). This sequentially analyses protocol was followed such that the same samples and spots could be studied. Note that samples were also collected for normal microbiological preservation methods (i.e., fixed in the field in glutaraldehyde), however, the thrust of the work presented in this paper was carried out on the untreated samples. The preserved samples were solely used for high-resolution microscopy and elemental analyses to cross-check the preservation or degradation of possible morphological biosignatures during sample transport and storage. Because the organic signatures from glutaraldehyde compromise the Raman analyses naturally only the untreated samples were analysed by Raman.

Raman spectroscopy

Spectra were recorded using a Renishaw *InVia* spectrometer with a Leica DMLM microscope and objectives with $\times 50$ and $\times 20$ magnifications. Two laser excitation wave-

lengths were used for the analyses (785 and 514 nm) in order to determine and quantify the differences between Raman signatures and to derive the best protocol for analyses of extant biosignatures. For each measurement, between 20 and 70 spectral accumulations at 10 seconds exposure time were recorded to improve signal-to-noise ratios. In addition, in order to avoid sample damage, low laser powers between 0.5 and 2.5 mW at source were used. Each layer was analysed with no further preparation being undertaken.

Scanning electron microscopy

Following the Raman analyses, the morphology and distribution of mineral phases and organic matter in the samples were imaged using a LEO 1530 Field-Emission Gun Scanning Electron Microscope (FEG-SEM). Qualitative elemental analyses were also carried out using an energy dispersive spectrometer (EDS) system that was attached to the FEG-SEM. With no further handling or preparation the samples were placed on an aluminium SEM stub and coated with a 3 nm platinum layer. Samples were inserted into the vacuum and imaging was done at an accelerating voltage of 3 kV and a working distance of 3 mm while EDS spot; analyses were carried out at 15 keV and a working distance of 8 mm. The samples that were preserved in the field in glutaraldehyde (in PO₄ buffer at pH 7) were sequentially dehydrated in an ethanol series (10, 30, 50, 70, 90 and 100 %) and imaged as described above. Critical point drying of the so prepared samples was unnecessary.

Results and discussion

Mineralogy

SEM-EDS shows that the dominant mineral in all layers was a calcium carbonate, which was identified as calcite based on the crystal morphology. Using Raman spectroscopy the calcium carbonate was confirmed as calcite, with bands at 1086, 712, 281 and 157 cm⁻¹. Several accessory minerals were also confirmed by Raman spectroscopic analyses, such as haematite, quartz, magnetite, graphite and anatase. Hematite was confirmed via the signatures at 224, 245, 296, 410 and 613 cm⁻¹, and it was present particularly in the yellowish layers. Quartz (Figure 2a), was identified based on bands at 204, 263, 353, 406, 508 and 1064 cm⁻¹, and its source was deemed to have been wind-borne dust (Figure 2b). Magnetite was detected in some spectra via a band at 664 cm⁻¹. SEM images also revealed the presence of various diatoms (Figure 2c) but a Raman signature for amorphous silica (opal A, broad bands expected at ~ 1100 and 800 cm⁻¹) was not identified. This is most probably due to the poorly ordered nature of the silica in opal A and its interference with other more crystalline Raman mineral signatures.

Table 1: Scytonemin Raman bands collected using 514 and 785 nm laser wavelength excitations.

Scytonemin (514)	Scytonemin (785)
1630 _s	1627 _{vw}
	1605 _{sh}
1599 _{vs}	1590 _{vs}
1591 _{vs,sh}	
1557 _s	1554 _s
1436 _m	1436 _s
1382 _m	1384 _{m-w}
1363 _{m-w}	
1323 _{m-w}	1320 _s
1282 _{m-w}	
	1278 _{m-w}
1250 _w	
	1242 _{m-w}
1171 _{vs}	1171 _{vs}
	1090 _w
1097 _m	
1023 _m	1023 _{vw}
985 _{vw}	982 _{m-w}
955 _w	
909 _{m-w}	908 _w
	886 _w
779 _{vw}	
	779 _w
764 _{vw}	
752 _{vw}	752 _{m-w}
677 _m	676 _m
660 _{m-w}	659 _w
640 _{vw-sh}	
629 _w	
576 _m	574 _m
538 _{vw}	
496 _{m-w}	495 _m
428 _{w-sh}	428 _{vw-sh}
441 _m	441 _{vw}
396 _{vw}	392 _w
306 _{vw}	

Graphite was present in several layers and it was characterised by a strong and sharp G Raman band at 1572 cm⁻¹ and a broader and weaker D band at 1308 cm⁻¹. The presence of graphite in the Troll springs is most probably related with aerosol transport from the antracite outcrops in the southern part of the island. Lastly, anatase, with bands at 637, 512, 394, 196 and 145 cm⁻¹, has been identified in several layers (Figure 3).

Biosignatures

Layers were analysed using the 785 and 514 nm laser excitation wavelengths and the organic signatures detected were assigned to scytonemin, carotene, chlorophyll and an unidentified organic compound (a porphyrin with a structure close to chlorophyll). It is important to highlight here that the Raman spectrum of scytonemin showed sig-

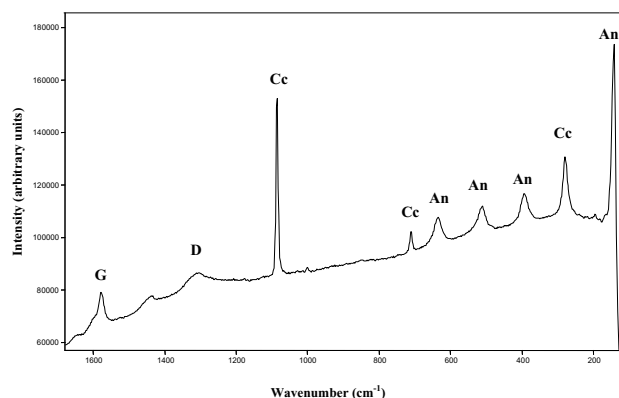


Figure 3

Raman spectrum of three minerals unambiguously identified by their Raman bands. Representative Raman spectrum of graphite (D 1308 cm⁻¹ and G 1572 cm⁻¹); anatase (An), with bands at 637, 512, 394, 196 and 145 cm⁻¹ and calcite (Cc), 1086, 712, 281 and 157 cm⁻¹ recorded at 785 nm laser wavelength. The broad band around 1400 cm⁻¹ could not be unambiguously assigned.

nificant variations in the relative intensity of the bands when recorded using the 785 or 514 nm laser excitation and this could lead to ambiguous pigment identification.

It is also noteworthy to point out the differences in organic component admixtures observed when using the different laser excitations on the same analyses spot. Several layers analysed with the 785 nm near infrared laser, revealed specific admixtures of pigments a) scytonemin and carotene, b) scytonemin, carotene and chlorophyll, c) carotene and chlorophyll. Conversely, at a 514 nm laser excitation wavelength the admixture of pigments detected on the same location was a) carotene and scytonemin and b) carotene only. In this study, carotene was never found on its own when using the 785 nm laser excitation but it always appeared with chlorophyll or scytonemin or both; however, using the 514 nm laser wavelength chlorophyll has not been identified in any of the spectra.

Raman signatures also give information about the degradation of organic compounds or the crystallinity of materials. For organic compound, the presence of sharp bands indicates, in general, that the molecules are not degraded; usually upon degradation the organic bonds become weaker, and the Raman bands appear broader; such a broadening indicates that the organic compounds have to some degree degraded. Similarly, for minerals broader Raman bands indicate lower levels of crystallinity.

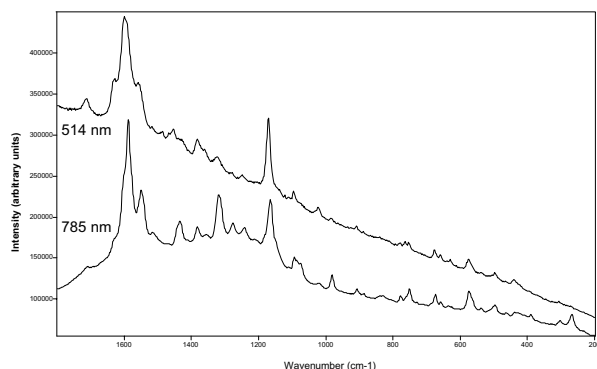


Figure 4
Representative Raman spectrum of scytonemin recorded at two different laser excitation wavelengths. The different relative intensities of the bands makes the compound identification difficult. For a more detailed comparison see Table 1.

Scytonemin

The spectra of scytonemin exhibit numerous Raman bands regardless if collected at 514 or 785 nm laser wavelength (Figure 4, Table 1). The most significant difference was observed in the relative intensities for specific bands when collected at the two laser excitations which was expressed in changes the overall appearance of the scytonemin spectra; this applied for both the corroborative Raman signatures as well as minor bands (Figure 4). Such differences could make a definitive compound identification difficult and this is specifically true if admixtures with other organics or minerals are present and band overlaps or interferences are observed.

For example (Table 1), the band at 1627 cm^{-1} was weak when the spectrum was collected at 785 nm, but at 514 nm the relative intensity increased and, moreover, the band shifted and appeared as a triplet at 1630 , 1599 and 1557 cm^{-1} . In addition, at 785 nm the strongest band was observed at 1590 cm^{-1} while with the 514 nm excitation this band shifted to 1599 cm^{-1} with a very strong shoulder at 1591 cm^{-1} ; lastly, in the spectrum collected using 785 nm laser wavelength, the strong band at 1554 cm^{-1} appeared at 514 nm as part of a triplet with medium intensity.

Another corroborative band for scytonemin can be found at 1320 cm^{-1} (medium intensity) but when the spectrum was collected with the 514 nm wavelength excitation the relative intensity of this band decreased significantly and the less significant signature at 1382 cm^{-1} , became stronger.

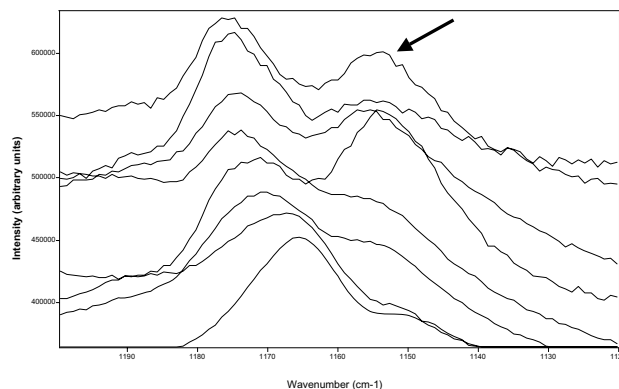


Figure 5
Stackplots of 8 scytonemin spectra recorded at 785 nm. The arrow shows the carotene band at around 1155 cm^{-1} , which is not related with the shift in scytonemin bands from 1172 cm^{-1} to 1165 cm^{-1} (marked by triangles), since no carotene is observed in the lower spectrum.

The spectral differences observed in the $1000\text{--}350\text{ cm}^{-1}$ region are not as significant as those in the $1800\text{--}1000\text{ cm}^{-1}$. Usually these bands are not used as corroborative signatures; however, distinct differences have been observed between the spectra collected using the two laser excitations (Figure 4, Table 1). For example, in the spectrum collected with 785 nm the band at 982 cm^{-1} showed a medium-weak intensity while at 515 nm this band appeared only as a very weak band. Some further differences were noted in the triplet at $779\text{--}764\text{--}752\text{ cm}^{-1}$ (514 nm laser), which became a band at 752 cm^{-1} with a very weak shoulder at 764 cm^{-1} and a weak signature at 779 cm^{-1} when the Raman spectrum was collected with the 785 nm laser excitation. Lastly, the weak band at 629 cm^{-1} with a shoulder at 640 cm^{-1} and the signature at 441 cm^{-1} with a shoulder at 428 cm^{-1} (using a 514 nm laser excitation wavelength), appeared just as very weak intensities in the spectrum collected using the 785 nm laser excitation.

Significative band shifts in scytonemin spectra

When the spectrum of scytonemin was collected using the 785 nm laser wavelength there were also significant shifts observed in the second main corroborative scytonemin band; according to the literature [24], the signature for this band should be centred at 1172 cm^{-1} but in this study we have observed that this band shifted from 1176 to 1165 cm^{-1} (Table 2 and Figure 5). It needs to be noted that this effect was not related to the presence of carotene (which exhibited a strong band centred about 1155 cm^{-1}). In Figure 5, stack plots of eight scytonemin spectra recorded in the region between $1200\text{--}1120\text{ cm}^{-1}$ are shown and only some of the spectra in this figure display the carotene signature (arrow in Figure 5). However, the spectrum with the lowest wavenumber for the prime scy-

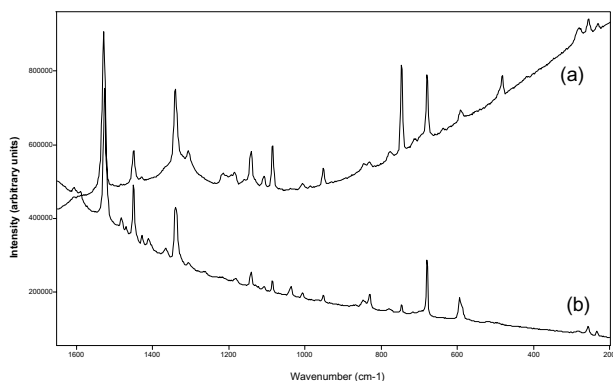


Figure 6

Spectra recorded of the chlorophyll-like compound using the (a) 785 nm and (b) 514 nm laser wavelengths. Important differences in relative intensities of the main corroborative Raman bands are shown. For more detailed information see Table 3 and text.

tonemin Raman band at $xxx\text{ cm}^{-1}$ (e.g., lowermost spectrum) does only reveal a small shoulder at $\sim 1150\text{ cm}^{-1}$ and this could be indicating the presence of carotene. The shift observed for this significant scytonemin Raman signature (lowermost to uppermost spectra from 1165 cm^{-1} to 1176 cm^{-1}) can thus not be attributed the carotene band overlap.

Although there is a minor shift in other strong scytonemin observed from 1555 to 1549 cm^{-1} (Table 2), the tendency to shift to a lower wavenumber was not as clear as the band at 1172 cm^{-1} and it is clearly not related with it, neither with the very strong signature between 1592 to 1589 cm^{-1} .

Chlorophyll and chlorophyll-like pigment

In several layers chlorophyll was identified using the 785 nm laser excitation by its Raman bands at 1625 , 1580 , 1436 , 1372 , 1323 , 1285 , 987 , 916 , 744 and 515 cm^{-1} . Note that, as mentioned above, chlorophyll was never identified using the green laser at 514 nm excitation wavelength.

Another organic compound, with a similar structure to chlorophyll (porphyrin), showed signatures at 1592 , 1530 , 1485 , 1451 , 1428 , 1411 , 1307 , 1216 , 1194 , 1144 , 1108 , 953 , 847 , 832 , 779 , 746 , 679 , 640 , 594 and 483 cm^{-1} and it was detected with both lasers in several layers. However, again differences in the Raman spectra collected with the two lasers (Figure 6, Table 3) were observed. The relative intensity of the corroborative signatures at 1339 cm^{-1} with a second band at 1307 cm^{-1} and the signature at 747 cm^{-1} was stronger in the spectrum collected with the

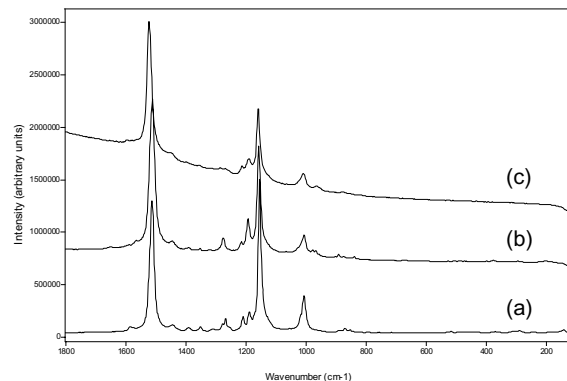


Figure 7

Representative Raman spectra of carotenoids found in the layers. (a) beta-carotene, (b) astaxanthin, (c) zeaxanthin/lutein, recorded at 514 nm laser wavelength. The carotene detection is easier with the 514 nm laser wavelength because of the resonance effect.

785 nm laser excitation in comparison with that collected using the 514 nm laser excitation. In addition, the medium intensity signature at 483 cm^{-1} , observed using the 785 nm excitation, was not detected when the Raman spectrum was collected with the 514 nm laser wavelength.

Carotenoids

Several different carotenoids have been identified by their Raman signatures (Figure 7). The mayor bands at 1508 , 1154 and 1005 cm^{-1} represent a carotene with a long chain structure and this could be assigned to astaxanthin. Another carotene exhibited bands at 1515 , 1155 and 1003 cm^{-1} and these are characteristic for beta-carotene while a third carotene, with the shortest chain length, showed Raman bands at 1522 , 1157 and 1007 cm^{-1} and these are assignable to zeaxanthin or lutein.

Morphological biosignatures

The microscopic imaging and spectral analyses of all layers showed that the main mineral in all layers was calcite. In addition, the presence of particles of dust, pollen grains and diatoms were discovered in some of the layers. EDS analyses of the mineral phases naturally showed C, O and Ca as peaks for the calcite substrate. In addition, sometimes Fe and Mn peaks were observed and these could be linked to the yellow-brown or white-pink layers.

However, the detailed study of all layers failed to locate any indication of clear and distinguishing morphological features that resemble bacteria, algae or fungi. The only organic looking structures found in some layers were fuzzy or diffuse structures and blebs of organic matter.

(Figure 8a and 8b). These features when analysed under the electron beam degraded fast, yet the EDS analyses showed a stronger C signal and sometimes a P signal when compared with the pure calcite substrate. Only in one case was one feature found that could be interpreted as a possible remnant of bacteria (Figure 8c).

The features in Figure 8a–c were initially discovered during the Raman analyses and they clearly showed Raman signatures for bona fide scytonemin and carotenoids. The same location was subsequently imaged and spectrally analysed using the FEG-SEM. Although the images clearly showed that the organic matter discovered had no morphological resemblance to microbes, it is also clear from the Raman spectra that this organic matter must have been microbial in origin. The Raman signatures on the globule shown in Figure 8a clearly demonstrated the presence and thus persistence and preservation of microbially derived scytonemin and carotenoids. As a test, we imaged and analysed a fresh sample from the edge of the active pool at the top of the terrace (see arrow in Figure 1) and clearly demonstrated that during the growth of the terraces abundant and diverse microbial communities as well as diatoms are present (Figure 8d) and that the biosignatures we documented in the fossil layers can only be derived from microbes that were present during growth of the sinter but that have been totally altered and degraded during aging.

Terrace evolution and preservation of organics

It is clear from the general aspect of the fossil part of the Troll springs that at some time the extent of the active part must have been much bigger than it is observed today. In addition, the multitude of large dry pools and their sizeable aprons, lips and draped sides (Figure 1a, b) indicate higher flow rates in the past when compared with the gentle sloped terraces that form in the present. Although it is not possible to provide an age of the various layers or of the terraces themselves, from calcite growth rate studies carried out in the active parts of the springs during a previous AMASE expedition [22,23] it is possible to roughly approximate an age for each individual layer and extrapolate to a possible age of the sequence studied here.

Hammer *et al* [22] (2006) estimated a maximum growth rate in the active springs of ~2 mm/year (minimum 0.1 mm/year). It has to be pointed out that this was done for slow growing sinters at temperatures between 12 and 23°C and under the assumption of continuous growth (over a one year period) and not taking into account seasonal variations, compaction due to later dehydration or aging. In addition, these variations in growth rates were strongly dependent and calcium carbonate saturation, which were in turn linked to water temperature (12–23°C) and depth (1–10 cm) as well as flow and evapora-

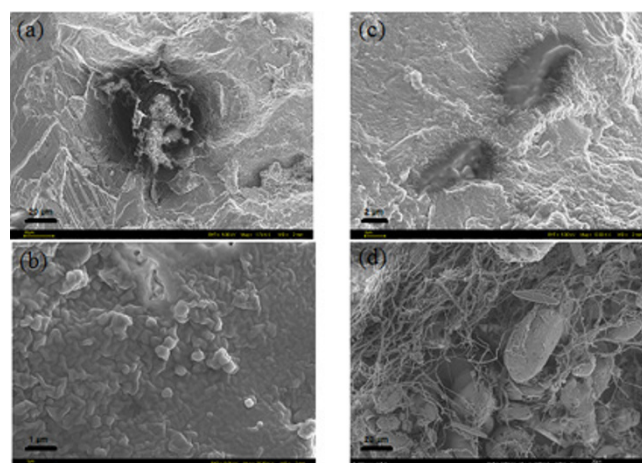


Figure 8

Representative FEG-SEM images of organic structures observed in the fossil terrace layers (a–c) compared to a fresh sinter rim sample from the active pool rim (d): (a) large organic matter cluster that showed no distinguishing morphological microbial features even at higher resolution (b). Only one structure could be interpreted as possible microbial remnants (c). All these structures when analyzed under EDS exhibited a stronger C peak than the calcite substrate; in addition these organic clusters were easily degraded under the electron beam (beam damage). For comparison (d) shows filamentous microbes in a sinter piece from the active part of the main terrace. Scales (a) and (d) 20 µm; (b) 1 µm; (c) 2 µm.

tion rate. Recently, Jamtveit *et al* [23] (2006) used spatially resolved isotopic measurements along a 5 cm piece of travertine collected from the middle part of the fossil terrace (see Figure 1 in this paper and Figure 2 in Jamtveit *et al* 2006). Their results showed that growth rates could be as high as 5.5 mm/year but they also tracked temperatures in the spring and surrounding air for 12 months and demonstrated that for about 6 months per year the springs are frozen. This will alter the overall growth rates because the cold temperatures will allow for no or only little growth to occur in the winter months and thus each year only a maximum of ~2.75 mm would be added to each layer.

Lastly, it is also important to note that certain parts of the terraces can become dry and others can be reactivated after prolonged dry periods (based on consecutive visits to the springs during 2003 to 2006 and historical records). Such drying out and subsequent reactivation of growth can lead to the formation of the observed gaps between layers (Figure 1b and 1c). When flow directions change and thus, for example an overflow dries this will lead to compaction and the formation of a harder crust. Once the same overflow becomes active again the next layer can grow. The observed gaps may also be affected by the past-presence of

Table 2: Scytonemin Raman band shifts collected in the eight studied layers at 785 nm laser excitation wavelength (SCY1 to SCY8 represent spectra in the eight studies progressively older layers). There is no relationship between the position of the individual scytonemin bands and the depth profile in the different layers and two different assignments may be present in the same layer or the same assignment may be valid in different layers.

SCY-1	SCY-2	SCY-3	SCY-4	SCY-5	SCY-6	SCY-7	SCY-8
	1630 _{vw}			1711 _w 1630 _{vw}	1711 _w 1629 _w	1711 _w 1629 _w	1711 _w
1627 _{vw}			1627 _{vw}				1624 _{vw} 1605 _{sh}
1605 _{sh}	1605 _{sh}	1605 _{sh}	1605 _{sh}	1605 _{sh}	1605 _{sh}	1603 _{sh}	
1592 _{vs}	1592 _{vs}	1591 _{vs}	1590 _{vs}	1590 _{vs}	1591 _{vs}	1590 _{vs}	1589 _{vs}
1555 _s	1555 _s	1552 _s	1551 _s	1554 _s	1554 _s	1551 _s	1549 _s
1436 _s	1436 _s	1435 _s	1436 _s	1436 _s	1436 _s	1436 _s	1435 _s
1385 _m	1384 _m	1385 _m	1385 _m	1384 _m	1384 _m	1383 _m	1383 _m
		1324 _s	1325 _s		1322 _s	1322 _s	1320 _s
1320 _s	1320 _s			1320 _s	1280 _{m-w}	1280 _{m-w}	1277 _{m-w}
				1278 _{m-w}	1245 _{m-w}	1249 _w	1243 _{m-w}
1176 _{vs}	1175 _{vs}	1174 _{vs}	1173 _{vs}	1171 _{vs}	1170 _{vs}	1167 _{vs}	1165 _{vs} 1095 _m
				1090 _w	1090 _m	1026 _{vw}	1024 _w
1024 _{vw}			984 _w	1023 _{vw}	1023 _w		
983 _w	983 _m	983 _m	910 _{vw}	982 _m	982 _m	983 _m	982 _m
909 _{vw}	909 _{vw}	909 _w		908 _w	908 _w	907 _w	908 _w
			890 _{vw}				
887 _{vw}	889 _{vw}	889 _w		886 _w	887 _w	887 _{vw}	887 _w
		778 _w		778 _{vw}	778 _w	779 _w	777 _w
754 _w	753 _w	752 _m	754 _m	752 _m	752 _m	752 _m	752 _m
677 _{vw}	680 _{vw}	676 _m	677 _m	676 _m	676 _m		

Table 2: Scytonemin Raman band shifts collected in the eight studied layers at 785 nm laser excitation wavelength (SCY1 to SCY8 represent spectra in the eight studies progressively older layers). There is no relationship between the position of the individual scytonemin bands and the depth profile in the different layers and two different assignments may be present in the same layer or the same assignment may be valid in different layers. (Continued)

					675 _m	675 _m
	662 _w					
		660 _w				
			659 _w	659 _w		
				637 _{vw}	658 _{vw}	658 _w
	578 _w				637 _{vw}	
			576 _m			
575 _w		575 _m				
			574 _m	574 _m	574 _m	574 _m
497 _{vw}	499 _{m-w}	497 _{m-w}			497 _w	497 _{m-w}
			495 _{m-w}	496 _{m-w}		
			495 _{m-w}	437 _w		
			392 _w	392 _w		
						390 _w

biological materials (i.e., exopolymer-rich biofilms) that would have dried up once water flow ceased. From the analyses of the modern equivalents of these fossil terraces, filamentous microbial colonies were observed in the fresh sinter pool edges (Fig. 8d) yet the observed gaps (Fig. 1b) can not be solely explained by biological processes and thus the drying and reactivation of sinter growth and compaction in the layers with time is the more likely cause for the observed layered structure of the terraces.

Based on these observations we determined a minimum and maximum possible growth rate for each layer in our traverse. The 8 layers studied varied in thickness between 7 and 18 mm and were distinguished by relatively large void spaces that indicated dry periods. If we take the previously determined growth rates (0.1 – 2.75 mm/year) and assuming that each layer grew in one continuous event, we can determine that the layers in our traverse could have taken between a minimum of 2.5 and a maximum of 180 years to grow.

However, it needs to be pointed out that the voids between the 8 layers in the traverse (Figure 1b and 1c), as well as the differences in density and porosity of each layer (Figure 1c) are all strong indication of prolonged dry periods between layer deposition. This naturally makes an estimate of the age of the whole sequence difficult. Based on our observations between 2003 and 2006 as well as historical evidence (i.e., Hoel and Høltedhal, 1911 and Banks et al 1998) we can infer that such dry periods may last between 2 and 20 years. Using a median growth rates for each layer of ~50 years we can estimate a ballpark upper maximum time for the growth of the studied 8-layer sequence of ~400 to 550 years. Such an estimate is

also supported by the fact that the last glaciation in the area was ~8000 years ago and that the springs must have been formed since that time, else they would have been eroded. Although no exact date for the ages of the fossil terraces is available the sequence studied here was collected from the oldest part of the terrace (Fig. 1a) and thus it is highly probably that there may have been no active flow for several hundreds of years. In addition, the lack of any evidence of endolithic or casmolithic signatures, support the fact that little to no biocolonisation of these sinters occurs since deposition. Note however, that the error in these age estimate are invariably large but the purpose of this calculation was solely to provide a possible upper time limit for the formation of the studied sinters. Combined with our Raman and SEM results that showed that specific microbially derived organic signatures have been preserved virtually unchanged in these old fossil terrace layers despite there being no clear indication of modern activity or clear remnant morphological biosignatures.

Conclusion

All geological layers show evidence of organic colonization with the presence of scytonemin, carotene, chlorophyll and/or chlorophyll-like compound, showing that a continuous colonization has occurred during the terrace formation. This confirms the observations of Hammer *et al*[22] (2006), who showed clear involvement of microbial communities in the build up of the new active terraces (see also Figure 8d). Here we showed, that Raman microspectroscopy in combination with SEM imaging and elemental analyses can be used to detect biological signatures that have been preserved for long periods of time even if remnant morphological evidence is missing. In addition, this can be done without chemical extraction

Table 3: Raman bands of the chlorophyll-like compound recorded with the 514 or 785 nm laser wavelengths. Note that the relative band intensities change significantly with the wavelength.

514 nm laser excitation	785 nm laser excitation
1592 _{vw}	1592 _{vw}
1530 _s	1530 _s
1485 _{m-w}	1485 _{vw}
1451 _s	1451 _m
1428 _w	1429 _w
1411 _w	
1339 _s	1341 _{vs}
1307 _w	1307 _m
	1219 _w
1194 _w	1194 _m
	1144 _{vw}
1108 _{vw}	1108 _{m-w}
1037 _{m-w}	
953 _{m-w}	952 _m
847 _{vw}	847 _{vw}
831 _m	831 _w
	779 _w
746 _{m-w}	746 _{vs}
680 _s	679 _s
	640 _{vw}
594 _m	591 _{m-w}
	483 _m
257 _{m-w}	257 _{m-w}
235 _w	235 _w
175 _w	175 _w

or sample handling. Our results showed that, in all layers, some of the colonizing organisms have produced scytonemin during their lifetime and each layer must have contained at least one of the scytonemin producing organisms. In addition, another type of microorganism which produced a chlorophyll-like compound was only found in one layer but it was detected using both laser wavelengths.

Although scytonemin has been detected with both laser excitation wavelengths the variations in relative band intensity strongly alters the appearance of the Raman spectra and this could make it difficult for unambiguous compound identification. The same problem was observed with the chlorophyll-like compound where some corroborative bands were absent when the spectrum was collected using 514 nm laser excitation.

It is relevant that although no morphological bacterial remains were found using SEM, the Raman spectra showed sharp bands indicating little to no pigment alteration; this indicates that although the original microbial community could not be observed via its morphological biosignatures and only organic matter has been preserved, the pigments themselves have been fully conserved. This is specifically interesting as these pigments have survived

in an environment with alternating dry and wet and cold and temperate periods over a long period of time. These results are particularly significant for planetary exploration since we showed that biosignatures could remain unaltered and thus remain preserved for decades to centuries. In addition, we show that their detection and quantification is possible by Raman spectroscopy, without any sample manipulation (except those derived of the exposition of a fresh surface for analysis by breaking the rock).

As Raman spectroscopy has been proposed as a part of a suite of analytical techniques for planetary exploration, particularly for Mars surface and subsurface future NASA and ESA missions [25-27] and both laser wavelengths tested in this study (and others like 532, 633 or 1065 nm) have been considered for miniaturised Raman spectrometers, the selection of the most adequate and most specific wavelength for organic detection is of prime significance. As we highlight in this study, the laser wavelength affects the relative intensity of the bands, making difficult the unambiguously identification of biosignatures. However, it is important to point out that the capability of detection of organic pigments could be compromised if the wrong laser wavelength is used.

The requirements for design of a miniaturised Raman spectrometer for planetary exploration should be related not only to its weight, robustness or other technical characteristics but also with the scientific aims of the research goals. In this respect, laser wavelength as well as spectral resolution or laser power are of vital importance for the success of the search for life missions to extraterrestrial planets. Naturally only when combined with microscopy, elemental or even isotopic analyses could extinct or extant biosignatures be unambiguously distinguished in fossil terrestrial and non-terrestrial environments.

Authors' contributions

SEJV and LGB together collected the samples during AMASE 2004, and carried out the SEM analyses and imaging. SEJV and HGME carried out the Raman analyses. SEJV, LGB and HGME have all equally contributed to writing the manuscript. The AMASE team has helped during the expedition with logistics and support.

All authors have read and approved the final manuscript.

Acknowledgements

We acknowledge the financial support from the Royal Society of Chemistry of London for SEJV and the funding from The University of Leeds for LGB without which this study would not have been possible. In addition, we are grateful to the expedition leader Hans Amundsen (PGP, University of Oslo) and other members of the 2004 Arctic Mars Analog Svalbard Expeditions ('AMASE') who contributed to this study through discussions and logistic support.

References

1. Diaz B, Schulze-Makuch D: **Microbial survival rates of *Escherichia coli* and *Deinococcus radiodurans* under low temperature, low pressure, and UV-Irradiation conditions, and their relevance to possible Martian life.** *Astrobiology* 2006, **6(2)**:332-347.
2. Cockell CS, Catling DC, Davis WL, Snook K, Kepner RL, Lee P, McKay CP: **The ultraviolet environment of Mars: biological implications past, present, and future.** *Icarus* 2000, **146(2)**:343-359.
3. Doran PT, Wharton RA, Des Marais DJ, McKay CP: **Antarctic paleolake sediments and the search for extinct life on Mars.** *J Geophys Res-Planet* 1998, **103(E12)**:28481-28493.
4. Knacke RF: **Possibilities for the detection of microbial life on extrasolar planets.** *Astrobiology* 2003, **3(3)**:531-541.
5. Cabrol NA, Grin EA: **A morphological view on potential niches for exobiology on Mars.** *Planet Space Sci* 1995, **43(1-2)**:179-188.
6. Clark BC: **Surviving the limits to life at the surface of Mars.** *J Geophys Res planets* 1998, **103(E12)**:28545.
7. Vago J, Gardini B, Kminek G, Baglioni P, Gianfiglio G, Santovincenzo A, Bayon A, Van Winnendael M: *Esa Bulletin-European Space Agency* 2006:16-23.
8. Bada JL, Sephton MA, Ehrenfreund P, Mathies RA, Skelley AM, Grunthaner FJ, Zent AP, Quinn RC, Josset JL, Robert F, Botta O, Glavin DG: *Astronom Geophys* 2005, **46(6)**:26-27.
9. Kminek G, Bada JL, Botta O, Glavin DP, Grunthaner F: **MOD: an organic detector for the future robotic exploration of Mars.** *Planet Space Sci* 2000, **48(11)**:1087-1091.
10. Schulze-Makuch D, Irwin LN: **Introduction to the special paper collection: methodologies and techniques for detecting extraterrestrial (microbial) life.** *Astrobiology* 2003, **3(3)**:487-488.
11. Ellery A, Ball AJ, Cockell C, Dickensheets D, Edwards HGM, Kolb C, Lammer H, Patel M, Richter L: **Vanguard--a European robotic astrobiology-focussed Mars sub-surface mission proposal.** *Acta Astronautica* 2005, **56(3)**:397-407.
12. Ellery A, Wynn-Williams DD: **Why Raman spectroscopy on Mars?--a case of the right tool for the right job.** *Astrobiology* 2003, **3(3)**:565-579.
13. Ellery A, Wynn-Williams DD, Parnell J, Edwards HGM, Dickensheets D: **The role of Raman spectroscopy as an astrobiological tool in the exploration of Mars.** *J Raman Spec* 2004, **35(6)**:441-457.
14. Villar SEJ, Edwards HGM: **Raman spectroscopy in astrobiology.** *Anal Bioanal Chem* 2006, **384(1)**:100-113.
15. Dickensheets DL, Wynn-Williams DD, Edwards HGM, Schoen C, Crowder C, Newton EM: *J Raman Spec* 2000, **31(7)**:633-635.
16. Moody CD, Villar SEJ, Edwards HGM, Hodgson PT, Doran JL, Bishop JL: *Spectroc Acta Pt A-Molec Biomolec Spectr* 2005, **61(10)**:2413-2417.
17. Edwards HGM, Villar SEJ, Parnell J, Cockell CS, Lee P: *Analyst* 2005, **130(6)**:917-923.
18. Villar SEJ, Edwards HGM, Cockell CS: *Analyst* 2005, **130(2)**:156-162.
19. Jorge Villar SE, Edwards HGM, Benning LB: *Icarus* 2006, **184**:158-169.
20. Edwards HGM, Moody CD, Newton EM, Jorge Villar SE, Russell MJ: *Icarus* 2005, **175(2)**:372-381.
21. Wynn-Williams DD, Edwards HGM: *Icarus* 2000, **144(2)**:486-503.
22. Hammer Ø, Jamtveit B, Benning LG, Dysthe DK: *Geofluids* 2005, **5**:140-150.
23. Jamtveit B, Hammer Ø, Andersson C, Dysthe DK, Heldmann J, Fogel ML: *Norwegian J Geol* 2006, **86**:387-395.
24. Edwards HGM, Garcia-Pichel F, Newton EM, Wynn-Williams DD: *Spectroc Acta Pt A-Molec Biomolec Spectr* 2000, **56(1)**:193-200.
25. [http://www.biocrawler.com/encyclopedia/ExoMars#Panoramic_instruments].
26. [http://www.esa.int/esaMI/Aurora/SEM6S8A5QCE_0.htm].
27. [http://nai.arc.nasa.gov/news_stories/news_detail.cfm?article=old_raman.htm].

Publish with **BioMed Central** and every scientist can read your work free of charge

"BioMed Central will be the most significant development for disseminating the results of biomedical research in our lifetime."

Sir Paul Nurse, Cancer Research UK

Your research papers will be:

- available free of charge to the entire biomedical community
- peer reviewed and published immediately upon acceptance
- cited in PubMed and archived on PubMed Central
- yours — you keep the copyright

Submit your manuscript here:
http://www.biomedcentral.com/info/publishing_adv.asp

